Theory of quantum spin Hall effect detection by measurements of the polarization resistance

Hui Zhang, Hua Jiang, X. C. Xie, and Qing-feng Sun

Phys. Rev. B **83**, 115402 — Published 3 March 2011

DOI: 10.1103/PhysRevB.83.115402

Theory of quantum spin Hall effect detection by measurements of the polarization resistance

Hui Zhang,[1] Hua Jiang,[2] X. C. Xie,[2,1,3] and Qing-feng Sun[1,*]
[1] *Institute of Physics, Chinese Academy of Sciences, Beijing 100190, China*
[2] *International Center for Quantum Materials, Peking University, Beijing 100871, China*
[3] *Department of Physics, Oklahoma State University, Stillwater, Oklahoma 74078, USA*

The detection of quantum spin Hall effect (QSHE) is investigated by using ferromagnetic leads as probes. A polarization resistance is introduced and it is defined as a voltage over a current, thus, can be measured with high precision like usual resistance. The polarization resistance exhibits the quantum plateau with the plateau value $h/2e^2$. In particular, this quantized plateau is found to be robust against both spin and normal dephasing effects. Furthermore, such robust feature of the plateau is insensitive to all experimental probing conditions and fluctuations, including type of probes, coupling strength, probing position, coupling means, fluctuation of magnetic flux. Therefore, the polarization resistance R_p can well reflect the topological nature of QSHE and it provides a direct and quantitative way to detect QSHE with high precision in an experiment.

PACS numbers: 73.43.-f, 72.80.Vp, 72.25.-b

I. INTRODUCTION

Being a topologically nontrivial state of matter, quantum spin Hall effect (QSHE) has gained great interest in the past few years. It was first introduced in graphene,[1] a monolayer hexagonal lattice of carbon atoms with a massless Dirac-like linear dispersion near the Fermi surface.[2] Soon after that, the prediction[3] in HgTe/CeTe quantum wells was made and the QSHE was observed in the experiment.[4] QSHE has many peculiar features due to the nontrivial property:[5] edges provide channels for electrons tunneling whereas the bulk remains insulated because that the spin-orbit coupling opens a band gap. In the view of band energy, there are two helical edge states crossing inside the bulk energy gap,[1,6] which means that electrons with opposite spin polarizations move along opposite directions at any given edge. Such helical edge states are topologically protected by time reversal symmetry and insensitive to disorder of the time reversal invariance since backscattering process is forbidden.[7] Therefore, it has greatly enlarged our understanding of nature and fundamental physics. Soon after the discovery of QSHE in two-dimensional system,[3,4] the topological insulator[8] in some three-dimensional material was also predicted in theory[9] and observed in experiments,[10] in which the movements of electrons are only permitted on the surface of the material. Generally speaking, the realization of a quantum spin Hall state requires spin-orbit coupling, as first realized in HgTe/CeTe quantum wells,[4] since QSHE is nontrivial with $\mathbb{Z}_2$ topological quantity[1] $\nu = 1$. Nonzero value $\nu = 1$ makes the obstructions necessary for wavefunctions within the effective Brillouin zone,[11] while it is not for an ordinary insulator which has $\nu = 0$. Very recently, an alternative way to realize QSHE is suggested in ferromagnetic (FM) graphene,[12] in which the system is CT invariant (here C and T respectively are the charge conjugation and time-reversal operation) rather than time reversal invariant. FM graphene has spin-resolved unique energy band with the linear dispersion relation for the low-energy carriers. In FM graphene, its carriers contain both electrons and holes, in particular, electrons and holes are completely spin-polarized with opposite spin polarization direction. Recently, some approaches have been suggested to realize the FM.[13,14] For example, the FM graphene can be realized by growing graphene on a FM insulator (e.g., EuO).[13] Based on such unique energy band of FM graphene and the split of spin-up and spin-down energy bands,[13,15] the CT-invariant QSHE can be realized. Specifically, when the Fermi energy E_F is tuned to between spin-resolved Dirac points, carriers with different spins will belong to different types (i.e., electron- and hole-like), accordingly QSHE occurs under an applied perpendicular magnetic field.

In order to detect the QSHE in experiments, some probing methods are applied and now the QSHE has been experimentally observed. The first try is to detect the induced spin accumulation on transverse boundaries with the use of Kerr rotation microscopy.[16] This method is indirect and qualitative, accordingly the quantized plateaus would not be obtained. The second way is to measure the longitudinal resistance.[4,5] Due to the helical edge states, the longitudinal resistance in QSHE system expects to be quantized with the quantum plateau value $h/2e^2$. But this quantum plateau can only survive in small-size sample (or mesoscopic sample) and it fails in macroscopic samples because of the spin dephasing. This is very different from quantum Hall effect. In the quantum Hall effect, the Hall resistance is measured and has the quantum plateaus. In particular, the quantum Hall plateaus are very robust against various impurity scattering as well as various dephasing effect,[17] and it can well survive in macroscopic sample. So it is urgent to find an observable physics quantity which can well reflect the topological nontrivial property of the QSHE, or in other words, this physical quantity exhibits the plateau which is robust against various dephasings and can sur-

vive in both mesoscopic and macroscopic samples. Recently we suggest and confirm that the quantized spin Hall resistance[18] R_s, the transverse spin bias over the longitudinal current, has the aforementioned characteristics. However, unlike the resistance, the high precision measurement of spin bias is hard to achieve experimentally. In fact, there is no efficient enough way to measure spin bias at the moment. Does there exist another approach to detect QSHE directly in both mesoscopic and macroscopic samples, where the observed quantity can reach high precision like the resistance and quantized plateaus can well hold in the presence of various dephasing processes?

In this paper, taking CT-invariant QSHE for example, the detection of QSHE is investigated in a four-terminal system by using FM probes. A polarization resistance R_p is introduced and it can well indicate the topological feature of QSHE. R_p is defined as the bias over current, so it can be measured with high precision in an experiment. The polarization resistance R_p versus the Dirac-point energy (or Fermi energy) exhibits the plateau with the plateau value $h/2e^2$. Specifically, the plateau can be robust against various dephasing effects so it can survive in macroscopic samples. Furthermore, we find that the robust feature of R_p is insensitive to type of probes, coupling strength between the probe and FM graphene, probing position, coupling means, fluctuation of magnetic flux *etc*. Noticeable, the topological feature of R_p is just due to the helical edge states in QSHE and it is independent on specific realizations, and accordingly the quantum plateau of R_p still exist and the way of detection is suitable for other types of QSHE as well.

The rest of this paper is organized as follows. In Sec. II we introduce our model and methods as well as ways of detection. In Sec. III we show numerical results of the polarization resistance R_p under dephasing effect which indicate topological feature of QSHE. Finally, Sec. IV gives the conclusion.

II. MODEL AND METHODS

We consider a four-terminal system consisting of a FM graphene ribbon coupled by two FM leads (the terminals 2 and 4) as shown in Fig.1(a). The FM terminals 2 and 4 are as the probes and they have the same polarization direction. The direction of polarization in FM graphene is assumed to be upward, but the FM terminals 2 and 4 can be spin-up or spin-down polarized corresponding to parallel or antiparallel with FM graphene respectively. In the parallel case, we let a small longitudinal current I flow from the terminal 1 through the central region to the terminal 3, and the FM terminals 2 and 4 are as the voltage probes with the voltage of FM terminal 2 denoted as V_P. In similar, in the antiparallel case, the voltage of the FM terminal 2 V_{AP} can also be obtained while a same longitudinal current I flows through the system which can be realized by using the constant current source. The polarization resistance R_p is then defined as $R_p \equiv (V_P - V_{AP})/I$. Furthermore, considering that V_P and V_{AP} are all voltages rather than spin bias, so the polarization resistance R_p can be measured in experiments at high precision like the usual resistance.

A four-terminal system is illustrated in Fig. 1(a). The FM graphene ribbon with width N is divided into three parts: the terminal 1, central region, and the terminal 3. The dephasing process is assumed to occur only in the central region whose length is N_c. The terminals 2 and 4 as the probes can be made of the usual FM leads (the square lattice) or FM graphene (the hexagonal lattice). In addition, an intermediate zone between the FM graphene ribbon and the probing terminal 2 (4) is introduced in order to avoid the spin-flip scattering in the contact of the probing terminals and FM graphene. The intermediate zone consists of the hexagonal lattice of the carbon atoms with the size $N_g \times N_p$. Besides, we also consider two coupling means between FM graphene and the probing terminals, where one has particle-hole symmetry (shown in Fig.1(a)) while the other one does not (shown in the inset of Fig.5(b)). In Fig.1(a) we show coupling mean with the particle-hole symmetry and the probing terminals are set in the middle of central region. In fact, the probing positions can be set anywhere along the boundaries.

In the tight-binding representation, the Hamiltonian of the aforementioned device is given by:[12]

$$\begin{aligned} H &= H_{\rm G} + H_{\rm P} + H_{\rm T} \\ H_{\rm G} &= \sum_{i\sigma}(\epsilon_d - \sigma M)c^\dagger_{i\sigma}c_{i\sigma} - t\sum_{\langle ij\rangle,\sigma} e^{i\phi_{ij}}c^\dagger_{i\sigma}c_{j\sigma} \\ H_{\rm P} &= \sum_{i\sigma}\epsilon_{p\sigma}a^\dagger_{i\sigma}a_{i\sigma} - t\sum_{\langle ij\rangle,\sigma} e^{i\phi_{ij}}a^\dagger_{i\sigma}a_{j\sigma} \\ H_{\rm T} &= -t_c\sum_{\langle ij\rangle,\sigma} e^{i\phi_{ij}}c^\dagger_{i\sigma}a_{j\sigma} + \text{H.c.} \end{aligned} \tag{1}$$

where H has been divided into three parts: $H_{\rm G}$, $H_{\rm P}$ and $H_{\rm T}$ corresponding to FM graphene ribbon, the FM probing terminals, hopping term between them respectively. In the above Hamiltonian, Fermion operator $c_{i\sigma}$ denotes the band states of FM graphene with on-site energy ϵ_d, spin $\sigma \in \{\uparrow, \downarrow\}$, and FM exchange field M, while $a_{i\sigma}$ with on-site energy $\epsilon_{p\sigma}$ is the same denotation in probing terminals. Here we assume that the FM probing terminals are completely polarized. Specifically, during the detection procedure, we set the spin-down coupling term in H_T to be 0 (i.e., $\Gamma_\downarrow = 0$) for parallel case and FM leads are spin-up polarized, whereas for the antiparallel case situation reverses. Moreover, we only consider the nearest neighbor hopping, and t is hopping element between the nearest neighbor sites, while t_c stands for the hopping element between FM graphene and probing terminals. In the presence of external perpendicular magnetic field B, there is an additional phase factor[12] adding to the hopping elements with $\phi_{ij} = \int_i^j \vec{A}\cdot d\vec{l}/\phi_0$ where $\vec{l} \equiv \vec{j} - \vec{i}, \phi_0 = \hbar/e$ and $\vec{A}$ is the vector poten-

tial. In our calculation, the magnetic field is described by the magnetic flux in a honeycomb lattice 2ϕ where $\phi \equiv (3\sqrt{3}/4)a^2B/\phi_0$ with a being the lattice constant of graphene.

There are two types of dephasing in realistic samples:[18] the first kind, which is called spin-dephasing process, makes carriers lose both phase and spin memories such as magnetic impurity induced spin-flip dephasing process, by contrast the normal dephasing process only induces the loss of phase memory for carriers such as electron-electron/phonon interaction. The influence of dephasing process can be simulated by using virtual-leads method.[19,20] The current flowing from lead p (including both real and virtual leads) can be calculated by using the multiprobe Landauer-Büttiker formula:[21,22]

$$I_{p\sigma} = \frac{e}{h}\int d\epsilon \sum_q T_{pq\sigma}(\epsilon) \times [f_{q\sigma}(\epsilon) - f_{p\sigma}(\epsilon)] \quad (2)$$

where $I_{p\sigma}$ is the current in terminal p (either real or virtual lead) with spin σ, and e and h are elementary charge and Planck constant respectively. $f_{q\sigma}(\epsilon) = 1/\{\exp[(\epsilon - \mu_{q\sigma})/k_BT] + 1\}$ is the Fermi distribution function in terminal q with chemical potential $\mu_{q\sigma}$ and temperature T. In Eq.(2), $T_{pq\sigma}(\epsilon)$ represents the transmission coefficient at energy ϵ, and it can be calculated through the equation $T_{pq\sigma} = \mathbf{Tr}[\Gamma_{p\sigma}G^r_\sigma\Gamma_{q\sigma}G^a_\sigma]$ where $\Gamma_{p\sigma}(\epsilon) = i[\Sigma^r_{p\sigma}(\epsilon) - \Sigma^a_{p\sigma}(\epsilon)]$ and Green's function $G^r_\sigma(\epsilon) = [G^a_\sigma(\epsilon)]^\dagger = \{\epsilon - H^C_\sigma - \sum_p \Sigma^r_{p\sigma}\}^{-1}$ with H^C_σ being the Hamiltonian of central region. For the real leads, the self-energy $\Sigma^r_{p\sigma}$ needs to be numerically calculated.[23] But for the virtual leads, $\Sigma^r_p = -i\Gamma_d/2$ where Γ_d denotes the dephasing strength. In the case of zero temperature, Eq. (2) is reduced to:

$$I_{p\sigma} = \frac{e^2}{h}\sum_q T_{pq\sigma}(V_{q\sigma} - V_{p\sigma}) \quad (3)$$

with $T_{pq\sigma} \equiv T_{pq\sigma}(E_F)$ and $V_{p\sigma}$ denoting the bias in terminal p with spin σ. Noticeable, $T_{pq\sigma}$ is the transmission coefficient for electrons tunneling from terminal q to terminal p with spin σ, and hereafter the Fermi energy is fixed at $E_F = 0$. Besides, $V_{p\sigma}$ is actually the spin-σ chemical potential in terminal p (i.e., $eV_{p\sigma} = \mu_{p\sigma}$).

In our simulation, a small longitudinal current I is applied between the terminals 1 and 3 and correspondence boundary conditions for the probing terminals 2 and 4 are $I_2 = I_4 = 0$. For virtual leads, however, there exists two kinds of boundary conditions corresponding to different dephasing types.[18] In the spin-dephasing case it has to be $I_i \equiv I_{i\uparrow} + I_{i\downarrow} = 0$ and $V_{i\uparrow} = V_{i\downarrow}$, while it is $I_{i\sigma} = 0$ in the normal dephasing case where i is the index indicting virtual leads and $\sigma \in \{\uparrow, \downarrow\}$. Thus, for the spin dephasing case the spin-up chemical potential is the same as spin-down chemical potential in all leads (either real or virtual), accordingly $V_{p\uparrow} = V_{p\downarrow}$. For the normal dephasing case, on the other hand, we have $V_{i\uparrow} \neq V_{i\downarrow}$ in usual for arbitrary virtual lead i. Finally, by using Eq. (3) and applying such boundary conditions, the voltage in the probing terminal 2 (V_P and V_{AP}) can be calculated, and so is the polarization resistance $R_p = (V_P - V_{AP})/I$.

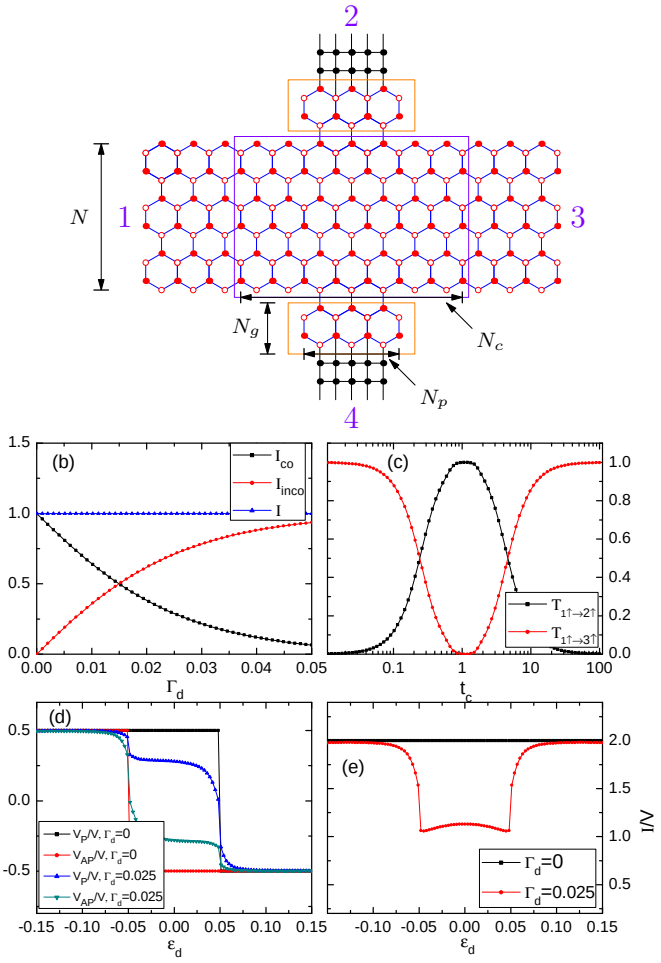

FIG. 1. (Color online) (a) illustration of four-terminal system consisting of a FM graphene ribbon coupled to two FM leads. In this diagram, the sizes of device are $N = 3, N_c = 7, N_g = 1$, and $N_p = 3$, and the FM leads couple to the middle of the central region. (b) shows changes of coherent component $I_{\rm co}$, incoherent component $I_{\rm inco}$, and total current I with increasing Γ_d for a two-terminal system at $\epsilon_d = 0$, and (c) presents the evolution of two specific tunneling coefficients $T_{1\uparrow\to2(3)\uparrow}$ with varying coupling strength t_c at $\epsilon_d = 0$. The measurements of $V_P/V, V_{AP}/V$ and I/V versus on-site energy ϵ_d in the spin dephasing case are plotted in (d) and (e) respectively for $\Gamma_d = 0$ and $\Gamma_d = 0.025$. Other unmentioned parameters in panels (b)-(e) are: $E_F = 0, N = 50, N_c = 31, N_g = 10, N_p = 17, M = 0.05, \phi = -0.02, t = 1, t_c = 1, \epsilon_{ps} = 0$. The probing terminals are FM leads and coupling position is in the middle of the central region.

III. NUMERICAL RESULTS OF POLARIZATION RESISTANCE UNDER DEPHASING EFFECT

Before discussing the polarization resistance R_p, let us first study the dephasing effect due to the virtual leads. Fig.1(b) shows the coherent component $I_{\rm co}$, incoherent component $I_{\rm inco}$, and total current I versus the dephasing strength Γ_d for a two-terminal system (decoupling the probing terminals 2 and 4). At around $\Gamma_d \simeq 0.015$, the so-called critical dephasing strength, $I_{\rm co}$ and $I_{\rm inco}$ are equal to each other so that current system length N_c is just equal to the phase relaxation length L_ϕ at the moment.[19] At $\Gamma_d \simeq 0.025$ we can see $I_{\rm co}$ is nearly half of $I_{\rm inco}$, accordingly N_c is almost two times of L_ϕ. In the following calculations, we use $\Gamma_d = 0.015$ as a typical dephasing strength in which the system is just at the verge of the mesoscopic and macroscopic sample, and use $\Gamma_d = 0.03$ as the strong dephasing regime, in which the system size is much longer than the phase relaxation length so that the system is the macroscopic sample.

When the probing terminals couple to the FM graphene ribbon, carriers can tunnel from the FM graphene terminal 1 to the probing terminals, which is shown in Fig.1(c). It can be seen clearly the transmission coefficient $T_{1\uparrow\to 2\uparrow}$ is nearly one while the coupling strength $t_c \simeq 1$. This means that in the case $t_c \simeq 1$ the contact between probing terminals and FM graphene ribbon is fine, i.e. in the strong coupling regime. On the other hand, while at around $t_c \simeq 0.1$ the transmission coefficient $T_{1\uparrow\to 2\uparrow}$ is about 0.1, and the system is in a weak coupling regime.

Now we take our calculations of V_P/V, V_{AP}/V as well as I/V, where $V = V_1 - V_3$ is the external voltage between the longitudinal terminals 1 and 3. Due to the unique energy band of FM graphene, there will be two types of carriers when $-M < \epsilon_d < M$. Specifically, the spin-up carriers are in the conduction band so that they are electron-like. Reversely, the spin-down carriers are hole-like since they are in the valence band. Because that electrons and holes have different moving directions under a perpendicular magnetic field (i.e., clockwise and anticlockwise) due to opposite Lorentz force, accordingly helical states occur at edges and also the QSHE is realized. In Fig. 1(d) and (e), we show the influence of spin-dephasing process on V_P/V, V_{AP}/V and I/V versus on-site energy ϵ_d. From Fig.1(d) and (e), we can see that within the QSHE regime ($-M < \epsilon_d < M$), both V_P/V and V_{AP}/V are spin-dependent since opposite spin-polarized carriers belong to different types and move in opposite direction. All V_P/V, V_{AP}/V, and I/V are strongly affected by the spin dephasing Γ_d, the difference between V_P/V and V_{AP}/V is reduced and I/V is dropped, because of the occurrence of the loss-phase spin-flipping scattering. On the other hand, while out of the QSHE regime ($\epsilon_d < -M$ or $\epsilon_d > M$), the spin-up and spin-down carriers will be the same type (electron- or hole-like) and accordingly they move in the same direction, thus V_P/V, V_{AP}/V and I/V remain invariant.

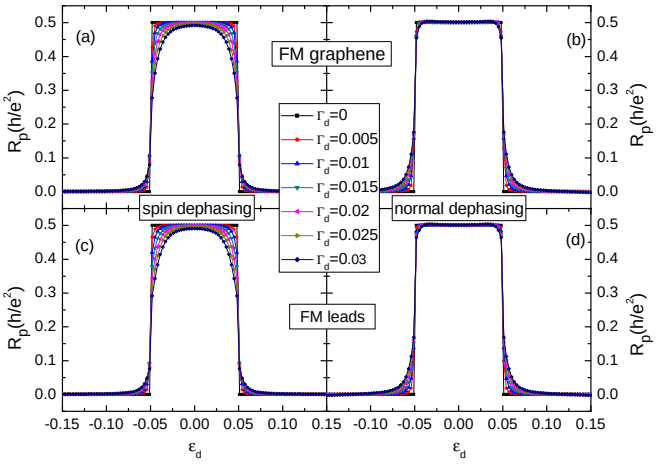

FIG. 2. (color online) Polarization resistance R_p versus energy ϵ_d for the FM-graphene probes (in panel (a) and (b)) and normal FM-lead probes (in panel (c) and (d)). The panels (a) and (c) are for the spin dephasing, while the panels (b) and (d) are for the normal dephasing. All unmentioned parameters are the same as in Fig.1.

Next we focus on the polarization resistance R_p ($R_p = (V_P/V - V_{AP}/V)/(I/V) = (V_P - V_{AP})/I$) and find out how the dephasing effect influences R_p. Fig. 2 shows the polarization resistance R_p versus the Dirac-point energy ϵ_d. Without the dephasing effect(i.e.: $\Gamma_d = 0$), the polarization resistance exhibits a quantum plateau in the QSHE regime $-M < \epsilon_d < M$ with the plateau value $h/2e^2$, because that opposite spin-polarized carriers belong to different types (electron- or hole-like) and move in opposite directions. While out of the QSHE regime, the polarization resistance is zero because now all carriers move in one direction. While in the presence of dephasing effect, as shown in Fig.2, the polarization resistance R_p well remains the quantized plateau even for very large dephasing strength Γ_d and also has nothing to do with probe types (either FM-graphene probe or normal FM-lead probe).

Specifically, the topological feature of R_p lies as follows. For the normal dephasing process, since the normal dephasing process cannot induce the spin flipping of the carriers, thus the carriers still well keep the direction of movement.[19] In fact, with varying Γ_d, values of V_P/V, V_{AP}/V and I/V are all maintained in this case. For the spin dephasing process, on the other hand, spin-flipping process makes a great contribution to the decrease of $V_P/V(V_{AP}/V)$ and I/V (see Fig.1(d) and (e)). Noticeable, these decreases occur simultaneously. Of more importance, such decreases are induced by the same spin-flipping process, so the polarization resistance R_p is expected to maintain its value with varying Γ_d due to its definition. In other words, R_p should have robust feature against both normal and spin dephasing processes. From Fig. 2(a) and (c) we can see R_p does remain quantized with varying dephasing strength Γ_d. Since the physical

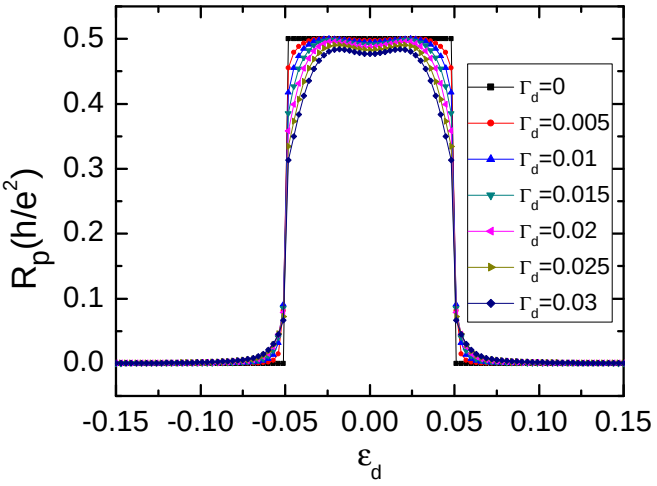

FIG. 3. (color online) R_p versus ϵ_d in the weak coupling regime $t_c = 0.1$ is shown. All unmentioned parameters are the same as in Fig.1.

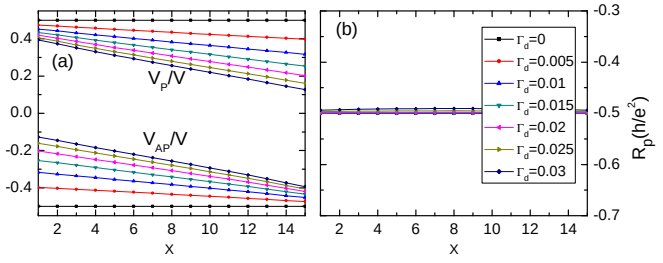

FIG. 4. (color online) (a) shows $V_P/V, V_{AP}/V$ versus probing position x along the upper boundary of FM graphene ribbon for different spin-dephasing strength Γ_d at fixed energy $\epsilon_d = 0$, while (b) shows changes of the polarization resistance R_p versus x. Other unmentioned parameters are the same as in Fig. 1.

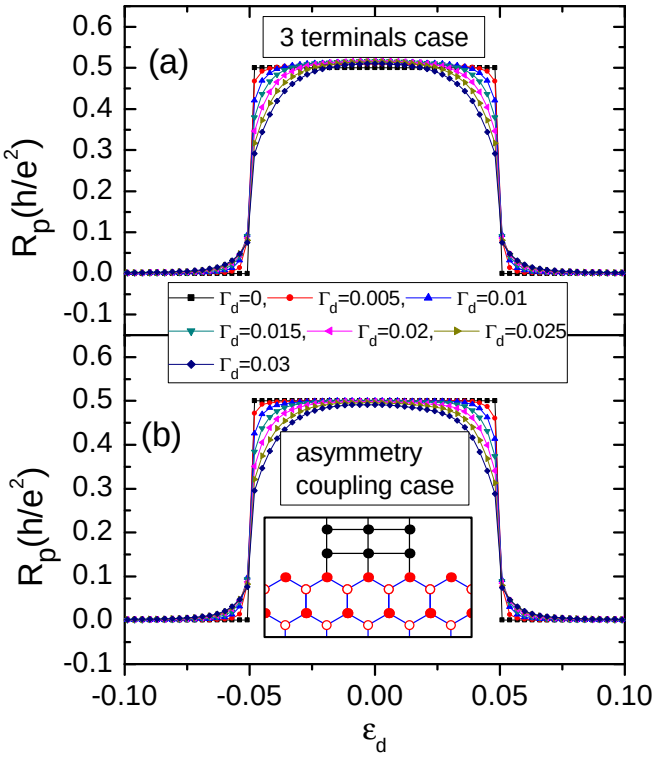

FIG. 5. (color online) The polarization resistance R_p versus energy ϵ_d for different spin-dephasing strength Γ_d under two coupling means of probing terminals: (a) is a three-terminal system now and the probing terminal only consists of terminal 2, and (b) is asymmetry-coupling probing case as shown in the inset of (b) where the particle-hole symmetry is broken at the moment. Other unmentioned parameters are the same as in Fig. 1(d).

picture of R_p in the normal dephasing case is simple and clear, thus only the influence of spin-dephasing process is considered in the following investigation.

In Fig. 3 we present R_p versum energy ϵ_d in the weak coupling regime $t_c = 0.1$, in which the different curves are for the different dephasing strength Γ_d. Here the quantized plateaus are clearly shown as well, in particular, this quantized plateaus can well survive even at the strong dephasing strength Γ_d. This is similar to the strong coupling regime at $t_c = 1$ shown in Fig.2(c). Noticeable, the coupling strength t_c in parallel and antiparallel cases can be different in experiments, but it also has little influence on the robust feature of R_p. In fact, in this situation all $V_P/V, V_{AP}$ and I are nearly independent on t_c. Therefore, this robust feature of R_p is independent on the coupling strength between FM graphene and probing subsystem.

So far, our probing terminals 2 and 4 have always been set in the middle of central region which means a π rotation symmetry resulting in that $T_{21\sigma} = T_{43\sigma}$. Following we study how is the effect of probing position (i.e. the coupling position of the probing terminals and FM graphene ribbon) on the robust feature of the plateau of polarization resistance R_p. In Fig. 4 we show measurable quantities V_P/V, V_{AP}/V as well as R_p versus the probing position along the upper boundary of FM graphene with varying Γ_d. First feature revealed in Fig.4(a) is the parallel voltage lines for any spin dephasing strengths. Besides, from Fig.4(b) one can see clearly that the polarization resistance R_p versus probing position x under different Γ_d merge into one single line indicating that R_p is insensitive to dephasing effect. And also, this line is parallel with horizontal axis which means little influence of probing position x on polarization resistance R_p.

Next, we adjust the coupling means of probing terminals and the FM graphene, and such numerical results are shown in Fig. 5. Here two specific coupling means are considered. In Fig. 5(a), it is a three-terminal system at the moment and the terminal 4 is decoupled. In the subfigure (b), we adjust the coupling way as illustrated in the inset. In this case particle-hole symmetry is not held any more. We find that, the polarization resistance R_p is insensitive to dephasing effect and always remain quantized with the plateau value $h/2e^2$ in either of the

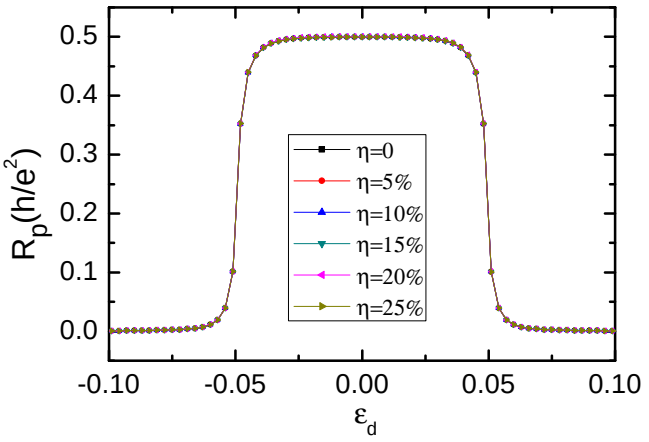

FIG. 6. (color online) The polarization resistance R_p versus energy ϵ_d for different fluctuations of magnetic field amplitude varying from 0 to 25%. It is in the spin dephasing case, and the dephasing strength is chosen as $\Gamma_d = 0.015$. Other unmentioned parameters are the same as in Fig. 1(d).

two cases. That's to say, such robust feature have nothing to do with specific coupling details between probing terminals and FM graphene ribbon.

Finally, we investigate the influence of various fluctuations on the quantum plateau $h/2e^2$ of polarization resistance R_p. As we know, in a real experimental setup the actual device parameters have inevitable fluctuations, such as the magnetic field amplitude (i.e., magnetic flux), device width and device length *etc*. Here we take the fluctuation of the magnetic field amplitude for instance and consider that the fluctuation only exist in the center region (see Fig.1a). While in the presence of the magnetic field fluctuation, the magnetic flux in each honeycomb lattice of the center region is $2\phi + \varphi_i 2\phi$, where φ_i is uniformly distributed in the range $[-\eta/2, \eta/2]$ with the fluctuation strength η. Fig. 6 shows the polarization resistance R_p versus energy ϵ_d with the fluctuation strength η varying from 0 to 25%. From Fig. 6, we can see that all curves almost overlap together and the plateau of R_p can well keep for the fluctuation strength η up to 25%. This is because of the system having the nontrivial topological property and the existence of the helical edge states. Also because of the nontrivial topological property and the existence of the helical edge states, the quantum plateau $h/2e^2$ of the polarization resistance R_p is robust against to other fluctuations (e.g. the device parameters N, N_c, N_p *etc*) and disorder.

IV. CONCLUSION

In summary, we investigate the detection of QSHE by using FM leads as probes. Taking CT-invariant QSHE for example, we define a polarization resistance R_p to indicate the topological feature of QSHE. Here R_p is defined as a voltage over a current, so it can be measured at high precision like the usual resistance. The polarization resistance versus the Dirac-point energy (or the gate voltage in the experiment) exhibits quantized plateau with the plateau value at $h/2e^2$. In particular, this quantized plateau is found to be robust against all dephasing effects (the normal and spin dephasing). Furthermore, the robust feature of the polarization resistance is also insensitive to all experimental probing conditions and fluctuations, such as type of probes, coupling strength, probing position, coupling means, fluctuation of magnetic flux *etc*. That's to say, the polarization resistance R_p can well indicate the topological nature of system, and it provides a direct and quantitative way to detect QSHE with high precision in experiments.

V. ACKNOWLEDGMENTS

This work was financially supported by NSF-China under Grants No. 10821403, No. 10974236, and No. 11074174, China-973 program, China Postdoctoral Science Foundation under Grants No. 19203 and US-DOE under Grants No. DE-FG02- 04ER46124.

* sunqf@iphy.ac.cn

[1] C. L. Kane and E. J. Mele, Phys. Rev. Lett. 95, 226801 (2005); Phys. Rev. Lett. 95, 146802 (2005).

[2] C. W. J. Beenakker, Rev. Mod. Phys. 80, 1337 (2008); A. H. Castro Neto, F. Guinea, N. M. R. Peres, K. S. Novoselov and A. K. Geim, Rev. Mod. Phys. 81, 109 (2009); A. K. Geim, Science 324, 1530 (2009); N. M. R. Peres, Rev. Mod. Phys. 82, 2673 (2010).

[3] B. A. Bernevig, T. L. Hughes, and S.-C. Zhang: Science 314, 1757 (2006).

[4] M. König, S. Wiedmann, C. Brüne, A. Roth, H. Buhmann, L. W. Molenkamp, X.-L. Qi, and S.-C. Zhang, Science 318, 766 (2007).

[5] M. KÖNIG, H. BUHMANN, L. W. MOLENKAMP, T. HUGHES, C.-X. LIU, X.-L. QI, and S.-C. ZHANG, J. Phys. Soc. Jpn 77, 031007 (2008).

[6] C. J. Wu, B. A. Bernevig, and S.-C. Zhang, Phys. Rev. Lett. 96, 106401 (2006).

[7] C. K. Xu and J. E. Moore, Phys. Rev. B, 73, 045322 (2006)

[8] M. Z. Hasan, C. L. Kane, arXiv. 1002.3895 (2010); S.-C. Zhang Physics. 1, 6 (2008); X.-L. Qi, and S.-C. Zhang, Physics Today 33 (2010); X.-L. Qi, and S.-C. Zhang, arXiv. 1008.2026 (2010); J. E. Moore Nature 464, 194 (2010)

[9] L. Fu and C. L. Kane, Phys. Rev. B 76, 045302 (2007); H. J. Zhang, C.-X. Liu, X.-L. Qi, X. Dai, Z. Fang, and S.-C. Zhang, Nature Physics 5, 438 (2009). L. Fu, C. L. Kane, and E. J. Mele, Phys. Rev. Lett. 98, 106803 (2007); J. E. Moore and L. Balents Phys. Rev. B 75, 121306(R) (2007).

[10] D. Hsieh, D. Qian, L. Wray, Y. Xia, Y. S. Hor, R. J. Cava, and M. Z. Hasan, Nature 452, 970 (2008); Y. L. Chen, J. G. Analytis, J.-H. Chu, Z. K. Liu, S.-K. Mo, X.-L. Qi, H. J. Zhang, D. H. Lu, X. Dai, Z. Fang, S.-C. Zhang, I. R. Fisher, Z. Hussain, Z.-X. Shen, Science 325, 178 (2009).

[11] L. Fu, 2009, Theory of Topological Insulators *PhD Thesis* University of Pennsylvania.

[12] Q.-f. Sun and X. C. Xie, Phys. Rev. Lett. 104, 066805 (2010)

[13] H. Haugen, D. Huertas-Hernando, and A. Brataas, Phys. Rev. B 77, 115406 (2008); J. Linder, T. Yokoyama, D. Huertas-Hernando, and A. Sudbø , Phys. Rev. Lett. 100, 187004 (2008).

[14] Y.-W. Son, M. L. Cohen, and S. G. Louie, Nature (London) 444, 347 (2006); E.-J. Kan, Z.Y. Li, J.L. Yang, and J. G. Hou, Appl. Phys. Lett. 91, 243116 (2007).

[15] Q. Y. Zhang, D. Y. Fu, B. G. Wang, R. Zhang, and D. Y. Xing, Phys. Rev. Lett. 101, 047005 (2008)

[16] Y. K. Kato, R. C. Myers, A. C. Gossard and D. D. Awschalom, Science 306, 1910 (2004); J. Wunderlich, B. Kaestner, J. Sinova and T. Jungwirth, Phys. Rev. Lett. 94, 047204 (2004).

[17] M. Kohmoto, Ann. Phys. 160, 343 (1985).

[18] H. Jiang, S. G. Cheng, Q.-f. Sun, and X. C. Xie, Phys. Rev. Lett. 103, 036803 (2009)

[19] Y. X. Xing, Q.-f. Sun, and J. Wang, Phys. Rev. B 77, 115346 (2008)

[20] M. Büttiker Phys. Rev. B 33, 3020 (1986).

[21] Y. Meir, N. S. Wingreen, Phys. Rev. Lett. 68, 2512 (1992)

[22] Electronic Transport in Mesoscopic Systems, edited by S. Datta (Cambridge University Press, Cambridge, England, 1995)

[23] D. H. Lee and J. D. Joannopoulos, Phys. Rev. B 23, 4997 (1981); M. P. López Sancho, J. M. López Sancho and J. Rubio, J. Phys. F: Met. Phys. 14, 1205 (1984); M. P. López Sancho, J. M. López Sancho and J. Rubio, J. Phys. F: Met. Phys. 15, 851 (1985).